remote sensing

MDPI

Article

Combining Spectral Data and a DSM from UAS-Images for Improved Classification of Non-Submerged Aquatic Vegetation

Eva Husson [1,*], Heather Reese [2] and Frauke Ecke [1,3]

1 Department of Aquatic Sciences and Assessment, Swedish University of Agricultural Sciences, SE-75007 Uppsala, Sweden; frauke.ecke@slu.se
2 Department of Forest Resource Management, Swedish University of Agricultural Sciences, SE-90183 Umeå, Sweden; heather.reese@slu.se
3 Department of Wildlife, Fish, and Environmental Studies, Swedish University of Agricultural Sciences, SE-90183 Umeå, Sweden
* Correspondence: eva.husson@slu.se

Academic Editors: Farid Melgani, Francesco Nex, Parth Sarathi Roy and Prasad S. Thenkabail
Received: 30 November 2016; Accepted: 1 March 2017; Published: 7 March 2017

Abstract: Monitoring of aquatic vegetation is an important component in the assessment of freshwater ecosystems. Remote sensing with unmanned aircraft systems (UASs) can provide sub-decimetre-resolution aerial images and is a useful tool for detailed vegetation mapping. In a previous study, non-submerged aquatic vegetation was successfully mapped using automated classification of spectral and textural features from a true-colour UAS-orthoimage with 5-cm pixels. In the present study, height data from a digital surface model (DSM) created from overlapping UAS-images has been incorporated together with the spectral and textural features from the UAS-orthoimage to test if classification accuracy can be improved further. We studied two levels of thematic detail: (a) Growth forms including the classes of water, nymphaeid, and helophyte; and (b) dominant taxa including seven vegetation classes. We hypothesized that the incorporation of height data together with spectral and textural features would increase classification accuracy as compared to using spectral and textural features alone, at both levels of thematic detail. We tested our hypothesis at five test sites (100 m × 100 m each) with varying vegetation complexity and image quality using automated object-based image analysis in combination with Random Forest classification. Overall accuracy at each of the five test sites ranged from 78% to 87% at the growth-form level and from 66% to 85% at the dominant-taxon level. In comparison to using spectral and textural features alone, the inclusion of height data increased the overall accuracy significantly by 4%–21% for growth-forms and 3%–30% for dominant taxa. The biggest improvement gained by adding height data was observed at the test site with the most complex vegetation. Height data derived from UAS-images has a large potential to efficiently increase the accuracy of automated classification of non-submerged aquatic vegetation, indicating good possibilities for operative mapping.

Keywords: digital surface model (DSM); drone; growth form; non-submerged aquatic vegetation; object-based image analysis (OBIA); Random Forest; remotely piloted aircraft system (RPAS); species identification; sub-decimetre spatial resolution; unmanned aerial vehicle (UAV); unmanned aircraft system (UAS)

1. Introduction

Unmanned aircraft systems (UASs) offer a potential data source for detailed surveying of aquatic vegetation with images having centimetre-level spatial resolutions [1]. At this high level of spatial

resolution, distinguishing structural details of individual plants is possible, for example, floating leaves on the water surface. In a previous study [2], we showed that a true-colour UAS-orthoimage with 5-cm pixels allowed for automated classification of growth-forms and six dominant taxa of non-submerged aquatic vegetation in a lake in northern Sweden. In the previous study, we used object-based image analysis and a Random Forest classification based on spectral and textural features. Using polygons as the spatial assessment unit, overall accuracies ranged from 56% to 83% for the growth-form level and from 52% to 69% for the dominant-taxon level. We found that classification accuracy decreased with increasing vegetation complexity. One main reason for misclassification was the confusion of taxa that appeared similar in the UAS-orthoimage, but belonged to different growth forms (emergent versus floating-leaved). While floating-leaved vegetation generally grows a couple of centimetres above the water surface, emergent plants can reach a considerable vegetation height, for example, 1–4 m for *Phragmites australis*, 1–3 m for *Schoenoplectus lacustris*, and 0.3–1.5 m for *Equisetum fluviatile* [3].

Several remote sensing methods are available which can provide three-dimensional (3D) data on surface and vegetation height, for example, LiDAR [4]. A method with a long tradition is stereoscopy that uses pairs of photographs of the same area taken from different positions to measure the height of objects on the Earth's surface [5]. Thanks to recent developments in digital photogrammetry and computer vision, in particular the Structure-from-Motion approach, dense 3D point clouds can be built directly from overlapping images, for example, from images taken from a UAS [6,7]. Cunliffe et al. [8] showed that this approach is able to resolve the vegetation structure even for small plants such as grasses and shrubs. A variety of software programs for UAS-image processing are available that can produce digital surface models [here called UAS-DSMs] and orthorectified image mosaics (here called UAS-orthoimages; [7]).

The majority of research on using height data in combination with spectral data for the classification of vegetation has been primarily made related to forestry (e.g., [9–11]). However, there are considerable differences in height and spatial extent between trees and aquatic plants. Reese et al. [12,13] studied the use of spectral data, elevation data (elevation above sea level, slope, and a wetness index), and 3D data from image matching (10 m × 10 m grid cells), as well as laser scanning (average point density of 1.4 m^{-2}) for low growing mountain vegetation classes including shrubs and grasses under 2 m in height. The overall classification accuracy increased with the inclusion of 3D data from both image matching and laser scanning compared to using spectral and elevation data alone. Gillan et al. [14] estimated the height of low-growing rangeland vegetation from aerial stereo images with 3-cm pixels and found a good correlation between field measurements and the vegetation height estimated from the images, even though the latter tended to be underestimated. Rampi et al. [15] combined LiDAR data (digital elevation model, DSM, compound topographic index, and intensity) and aerial imagery to map wetlands versus other land cover types in three ecoregions with an object-based image analysis approach and achieved high classification accuracies (>90%).

Height data derived from UAS-images, in most cases with Structure-from-Motion software, has been used, for example, for landslide detection [16] and segmentation of buildings [17]. Lechner et al. [18] mapped the vegetation extent of upland swamps surrounded by eucalyptus woodland in Australia. The UAS was equipped with two cameras to record the visible and infrared spectrum with a resolution of 4 cm. A UAS-DSM derived from the infrared images was used for an initial classification which was then refined using spectral information from true-colour UAS-images, among other parameters. Kuria et al. [19] analysed seasonal vegetation changes in a Tanzanian wetland, based on 0.8 m spatial resolution true-colour image data acquired with a UAS, a DSM derived from UAS-images, and commercial radar data. Thirteen land cover classes were identified, including several classes with emergent aquatic vegetation. The land cover classes were then combined to five generalized classes which showed an overall accuracy of ~90% for two analysed seasons [19]. Tamminga et al. [20] used a true-colour UAS-orthoimage with 2.5-cm pixels to map geomorphic and aquatic habitat features for river management. In addition to the mapping, a digital elevation model derived from the UAS-images was used for hydrodynamic modelling of water depth and velocity.

Boon et al. [21] delineated wetlands and assessed wetland vegetation health in South Africa based on a true-colour 1.8-cm spatial resolution UAS-orthoimage in combination with height data from 3D point clouds (3.8-cm resolution in the wetland area and 29-cm resolution in the surrounding area). They found that the inclusion of height data significantly enhanced wetland delineation and classification. These studies demonstrate that height data can contribute critical information in the classification process and have the potential to increase classification accuracy as compared to the use of spectral data from UAS-images alone.

In this study we test the hypothesis that the inclusion of height data derived from overlapping UAS-images in the form of a UAS-DSM in addition to spectral and textural features from a UAS-orthoimage increases the classification accuracy of non-submerged aquatic vegetation at two levels of thematic detail: (a) Growth forms and (b) dominant taxa in comparison to a classification which only used spectral and textural features from the UAS-orthoimage [2]. In particular we expect that the confusion between taxa that appear spectrally similar in the UAS-orthoimage, but belong to different growth forms, will be reduced.

2. Materials and Methods

2.1. Study Area, Image Acquisition, Test Sites, and Aquatic Plant Taxa

Lake Ostträsket (64°55′N, 21°02′E) is a boreal lake in northern Sweden with a surface area of 1.8 km^2 [2]. The littoral zone of the lake was surveyed with a miniature fixed-wing aircraft of the type flying wing, the Personal Aerial Mapping System (PAMS) by SmartPlanes AB (Skellefteå, Sweden), in August 2011 [2]. The PAMS was equipped with an off-the-shelf Canon Ixus 70® digital compact camera (Canon Inc., Tokyo, Japan) with a seven megapixel sensor and an RGB colour filter (380–750 nm). The camera was fitted into the body of the aircraft and collected nadir image data. The flying height of 150 m resulted in a ground sampling distance of 5.6 cm. The along- and across-track image overlap was set to 70%. A true orthoimage was produced by an external image provider with Inpho® software (INPHO GmbH, Stuttgart, Germany) based on a high resolution surface model with a grid size of 30 cm derived from a dense point cloud (100–400 points per m^2) and was georeferenced using ground control points identified in aerial photographs from the Swedish National Land Survey (spatial resolution 0.5 m). The internal planar precision of the orthoimage (i.e., the relative errors within individual photo blocks) was 4–5 cm and the internal height precision was 8–9 cm. The pixel size of the produced orthoimage was 5 cm. More details on PAMS, the camera, weather conditions, and orthoimage production can be found in Husson et al. [2]. From the resulting true-colour UAS-orthoimage with 5-cm pixels, five test sites (100 m × 100 m each) were selected [2]: four sites represented the natural variability of the lake with varying vegetation complexity (proportion of mixed vegetation stands, vegetation cover and density, and taxa composition). Vegetation complexity increased from Site I to Site IV. At Site I there were mainly single-taxa stands surrounded by open water. Site IV was almost entirely covered by mixed vegetation. At the fifth test site, the UAS-orthoimage had poor image quality caused by a combination of wave action, blur, specular reflection of clouds, and sunglint. This test site showed medium vegetation complexity and was included to test the classification robustness given poor image quality. Non-submerged aquatic plant taxa present at Lake Ostträsket include helophytes (i.e., emergent taxa: *Equisetum fluviatile*, *Schoenoplectus lacustris*, and *Phragmites australis*) as well as nymphaeids (i.e., floating-leaved taxa: *Potamogeton natans*, *Sparganium* spp., and *Nymphaea*/*Nuphar* spp.; [2], Figure S1). Sparse and dense stands of *E. fluviatile* looked very different and were therefore divided into two classes: sparse stands of *E. fluviatile* having 10%–50% area coverage (from now on called "sparse *E. fluviatile*") and dense stands of *E. fluviatile* having >50% area coverage (from now on called "dense *E. fluviatile*"; [2]). Not all taxa were present at all test sites (Table 1). More details on Ostträsket, the five test sites, and the vegetation can be found in Husson et al. [2].

Table 1. Taxa present at each test site given in order of decreasing area in which the respective taxon was dominant (i.e., it was the taxon with the highest % cover).

Site	Taxa
I	*Schoenoplectus lacustris*, *Nymphaea/Nuphar* spp., *Equisetum fluviatile* (dense), *E. fluviatile* (sparse), *Potamogeton natans*, *Sparganium* spp.
II	*S. lacustris*, *Nymphaea/Nuphar* spp., *P. natans*, *Sparganium* spp., *E. fluviatile* (sparse), *E. fluviatile* (dense)
III	*Nymphaea/Nuphar* spp., *E. fluviatile* (sparse), *E. fluviatile* (dense), *P. natans*, *Sparganium* spp.
IV	*Phragmites australis*, *S. lacustris*, *P. natans*, *Nymphaea/Nuphar* spp., *E. fluviatile* (dense), *E. fluviatile* (sparse)
V	*S. lacustris*, *P. natans*, *P. australis*, *Nymphaea/Nuphar* spp.

2.2. Height Data

Point cloud data from which vegetation height was determined for the five test sites was derived from the original overlapping single UAS-images using the Structure-from-Motion software PhotoScan® (Professional edition, v. 1.2.4, Agisoft LLC, St. Petersburg, Russia), because the original UAS-DSM from the orthoimage production by the external image provider was not available for this study. For each test site, the images of the respective flight block and the camera positions recorded during image acquisition were loaded into PhotoScan®. The user-specified accuracy of the camera coordinates was set to 10 m. Blurred images were excluded from the dataset and the images were aligned (accuracy: high; pair preselection: reference; key point limit: 40,000; tie point limit: 4000). Points with low image count ($\leq$2), high reprojection error ($\geq$0.45), and low projection accuracy ($\geq$40) were deleted. Camera alignment optimisation was then run in PhotoScan® and the surface was reconstructed (building of mesh (face count: low) and texture). Ground control points with coordinates measured in the field were not available for our study. To minimize the displacement of the DSM compared to the orthoimage which was georeferenced from the beginning, 12–25 reference points per test site were selected in the orthoimage and manually placed as markers for georeferencing in PhotoScan®. The reference points were evenly distributed throughout the whole test site with additional reference points at the corners and in the centre of the image. The user-specified accuracy of the reference points was set to 0.005 m in PhotoScan. We manually added reference points until the total XY error (average mean square error) of the reference points reached a minimum, indicating that the displacement between the DSM and the orthoimage was at a minimum. The displacement (i.e., the total XY error) at the five test sites was $\leq$5.6 cm. We did not have any field-based height measurements for these points. Therefore, we selected reference points at the water surface, mainly floating leaves, and assigned a value of zero as the height. Since we used the water surface as the zero height level we also subtracted 15 m from the z-values of the recorded camera positions because Lake Ostträsket is located at 15 m above sea level. When the markers were placed, a dense point cloud was produced (quality setting: high; depth filtering: mild) that was used to build a DSM (Figure 1). Due to the movement of waves and since the UAS-images were not taken simultaneously, image matching was difficult for open water surfaces and some sparse vegetation stands at Site V in regions with poor image quality. We therefore disabled interpolation for the DSM production. Initial tests showed that DSMs produced with interpolation displayed unreasonably high and/or low height values in areas with open water. By disabling interpolation, the areas with unreasonable height values could be reduced. The produced DSMs for the five test sites had a ground sampling distance of ~9 cm and a point density of $\geq$106 points per m^2. The UAS-DSMs were exported as GeoTiff-files with a pixel size of 5 cm in order to match the pixel size of the UAS-orthoimage.

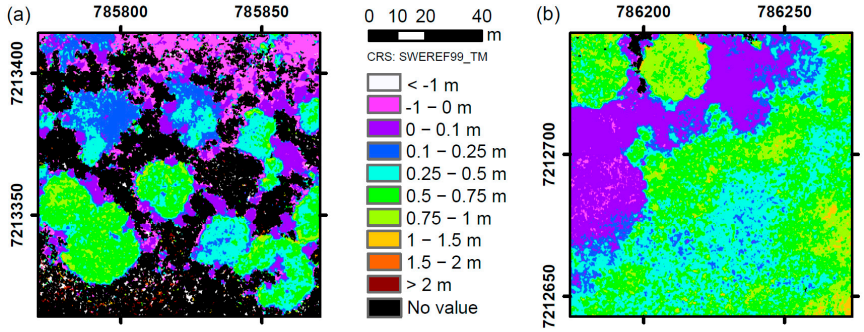

Figure 1. Examples of produced digital surface models for test site I (**a**) and test site IV (**b**).

2.3. Object-Based Image Analysis and Accuracy Assessment

Object-based image analysis in combination with Random Forest classification was applied to the five test sites using the software eCognition Developer® (v. 9.1, Trimble Germany GmbH, Munich, Germany). In the current study, we performed the Random Forest classification on the growth-form and the dominant-taxon level based on spectral and textural features from the UAS-orthoimage as described in Husson et al. [2] with the only difference being that the UAS-DSM was loaded as an additional image layer in eCognition® and a new feature for classification was added: "Mean DSM" (i.e., the mean height value for each segment). The growth-form level included three classes: Water, nymphaeid, and helophyte. For the classification at the dominant-taxon level, the water area was masked out [2]. We defined the dominant taxon as the taxon that covered the largest area in the respective vegetation stand. Seven classes were included according to the dominant taxa given in Table 2. To ensure full comparability between the current study and Husson et al. [2], the segments from Husson et al. [2] obtained by "Multiresolution Segmentation" based on the UAS-orthoimage alone, were used. For each test site, 40 training sample-segments per class were randomly selected from the sites' "Reference Maps" which were manually produced with visual interpretation. More details on the production of the Reference Maps are provided in Husson et al. [2], including the classification scheme for visual interpretation with image examples for all taxa in the Supplementary Materials. At Site I, we selected only 30 training samples per dominant taxa class because there were two classes with a low total number of segments (59 and 60 segments; [2]). The training sample-segments used in both studies were identical. Also, for accuracy assessment we used exactly the same validation sample-segments as in Husson et al. ([2]; i.e., 350 randomly selected sample-segments per site). In cases where a class was represented by only a few segments, we randomly selected more samples so that there were at least ten segments for that class [2]. To evaluate the classification, a segment-based error matrix was produced. We calculated overall, Producer's, and User's accuracy, Cohen's Kappa coefficient [22], as well as overall quantity disagreement and overall allocation disagreement [23]. Producer's accuracy is the probability that a polygon belonging to a given category on the ground has also been labelled that category in the map while User's accuracy is the probability that a polygon classified into a given category actually represents that category on the ground. The Kappa statistic takes into account the fact that even assigning labels at random results in a certain degree of accuracy. The Kappa coefficient has however been criticised as being misleading and redundant in remote sensing applications [23,24]; for this reason we have also included quantity and allocation disagreement as an alternative to Kappa [23]. Overall quantity disagreement is defined as the difference between two data sets due to an imperfect match in proportions of the mapped categories. Overall allocation disagreement is defined as the difference between two data sets due to an imperfect match between the spatial allocations of the mapped categories. Since the validation sample-segments varied in size, we also produced an area-based error matrix (related to the number of pixels inside the selected validation segments) and calculated the overall, Producer's, and User's accuracies to evaluate the map's usability by assessing the correctly classified area as proposed by Radoux et al. [25].

Table 2. Overall classification accuracy (%, segment-, and area-based), Cohen's Kappa coefficient, overall quantity disagreement (%), and overall allocation disagreement (%) for the classification based on height data combined with spectral and textural features for test sites I–V presented by the level of thematic detail (growth forms and dominant taxa). For comparison, the results from our previous study [2] based on spectral and textural features alone were reproduced in this table. Bold numbers indicate a statistically significant difference with the inclusion of height data ($N = 5$, $\alpha < 0.05$).

Level of Thematic Detail	**Growth Forms**					**Dominant Taxa**				
Site	**I**	**II**	**III**	**IV**	**V**	**I**	**II**	**III**	**IV**	**V**
Overall accuracy (segment-based)										
Height, spectral, and textural features	84.6	87.1	78.9	77.7	78.0	79.1	81.1	66.4	81.9	85.4
Spectral and textural features	80.3	83.4	74.3	56.3	63.4	68.6	64.7	63.0	52.2	65.4
Difference	**4.3**	**3.7**	**4.6**	**21.4**	**14.6**	**10.5**	**16.4**	**3.4**	**29.7**	**20.0**
Overall accuracy (area-based)										
Height, spectral, and textural features	94.7	92.9	82.3	76.6	74.3	82.7	85.3	63.2	82.1	86.2
Spectral and textural features	93.6	91.6	77.8	56.4	64.8	72.7	70.3	61.0	51.8	74.6
Difference	**1.0**	**1.2**	**4.5**	**20.2**	**9.5**	**9.9**	**15.0**	**2.3**	**30.2**	**11.7**
Cohen's Kappa coefficient										
Height, spectral, and textural features	0.75	0.76	0.58	0.54	0.64	0.68	0.67	0.38	0.74	0.81
Spectral and textural features	0.69	0.69	0.51	0.25	0.40	0.54	0.46	0.34	0.39	0.54
Difference	**0.07**	**0.07**	**0.07**	**0.29**	**0.24**	**0.14**	**0.21**	**0.04**	**0.35**	**0.27**
Overall quantity disagreement										
Height, spectral, and textural features	6.9	6.9	11.1	18.6	11.4	10.7	10.8	20.7	13.5	6.0
Spectral and textural features	8.0	7.4	14.6	36.3	10.9	14.6	23.1	22.7	30.8	2.9
Difference	−1.1	−0.6	−3.4	−17.7	0.6	−3.9	−12.2	−2.0	−17.3	3.1
Overall allocation disagreement										
Height, spectral, and textural features	8.6	6.0	10.0	3.7	10.6	10.2	8.1	12.9	4.7	8.6
Spectral and textural features	11.7	9.1	11.1	7.3	25.7	16.8	12.2	14.3	17.0	31.7
Difference	**−3.1**	**−3.1**	**−1.1**	**−3.7**	**−15.1**	**−6.6**	**−4.2**	**−1.4**	**−12.4**	**−23.1**

2.4. Statistical Analysis

We used non-metric, one-sided Wilcoxon matched pairs signed-rank tests [26] at both levels of thematic detail to test for a potential increase in classification accuracy due to incorporation of height data. In other words, we compared the results from our previous study which were based on spectral and textural features from the UAS-orthoimage only [2], to our new results which were based on spectral and textural features from the UAS-orthoimage and height data from the UAS-DSM. For overall accuracy (both segment- and area-based), Kappa, overall quantity disagreement, and overall allocation disagreement, the sample size N was five and we used a significance level of $\alpha < 0.05$. We also compared the Producer's and User's accuracies (both segment-, and area-based) with and without height data at each level of thematic detail for all classes and sites combined. Here the sample size was larger ($N = 15$ for growth forms and $N = 27$ for dominant taxa) and we used three significance levels, namely * for $\alpha < 0.025$, ** for $\alpha < 0.005$, and *** for $\alpha < 0.0005$. For the statistical analysis we used Statistica® software (v. 13, Dell Inc., Tulsa, OK, USA).

3. Results

The use of height data combined with spectral and textural features resulted in better classification results at all test sites, as compared to using spectral and textural features alone. The increase in overall accuracy (segment- and area-based) was statistically significant at both levels of thematic detail ($T_5 = 0$, $p = 0.043$ for all four tests).

At the growth-form level, the use of height combined with spectral and textural features gave an overall accuracy of 78%–87% (segment-based). For the five test sites, this represented an average increase of 10% (range 4%–21%, Table 2). The increase in accuracy was largest at Sites IV and V (Table 2). The correctly classified area after the inclusion of height data was 74%–95% (Table 2, area-based overall accuracy). For the five test sites, this represented an average increase of 7% (range 1%–20%, Table 2).

At the dominant-taxon level, the use of height data combined with spectral and textural features gave an overall accuracy of 66%–85% (segment-based). For the five test sites, this represented an average increase of 16% (range 3%–30%, Table 2). The correctly classified area after the inclusion of height data was 63%–86% (Table 2, area-based overall accuracy) which represented an average increase of 14% for the five test sites (range 2%–30%, Table 2). The largest increase (30%) in overall accuracy (segment- and area-based) was observed at Site IV (Table 2, Figure 2e,f), which was the site with the most complex vegetation and that showed the lowest overall classification accuracy in the study without height data [2]. In comparison to the other test sites, the increase at Site III was small (3% in the segment-based and 2% in the area-based assessment; Table 2). The orthoimages and produced vegetation maps for dominant taxa at Sites I, II, IV, and V are included in Figure 2.

Kappa increased for all test sites when the height data were added (Table 2). At both levels of thematic detail the increase of Kappa was statistically significant ($T_5 = 0$, $p = 0.043$ for both tests). Overall quantity disagreement increased slightly at Site V (Table 2), but decreased at all other sites (Table 2), however, the difference was not statistically significant (growth-form level: $T_5 = 1.5$, $p = 0.110$; dominant-taxon level: $T_5 = 2.0$, $p = 0.140$). Overall allocation disagreement decreased significantly at all test sites and levels of thematic detail (Table 2; $T_5 = 0$, $p = 0.043$ for both levels of thematic detail). At both levels of thematic detail, the overall quantity disagreement was larger than the overall allocation disagreement at the majority of sites. Complete error matrices for both levels of thematic detail at all test sites and differences between error matrices from the classifications with and without height data are included in the Supplementary Material (Table S1).

Producer's and User's accuracies at the growth-form level increased by including height data for the majority of classes and sites (Table 3), and the overall increases of segment- and area-based Producer's and User's accuracies were statistically significant (T and p values given in Table 3). The largest increases were observed for the classes of nymphaeid and helophyte at Sites IV and V (Table 3). For water, Producer's and User's accuracies were only marginally affected by the inclusion of height data (Table 3).

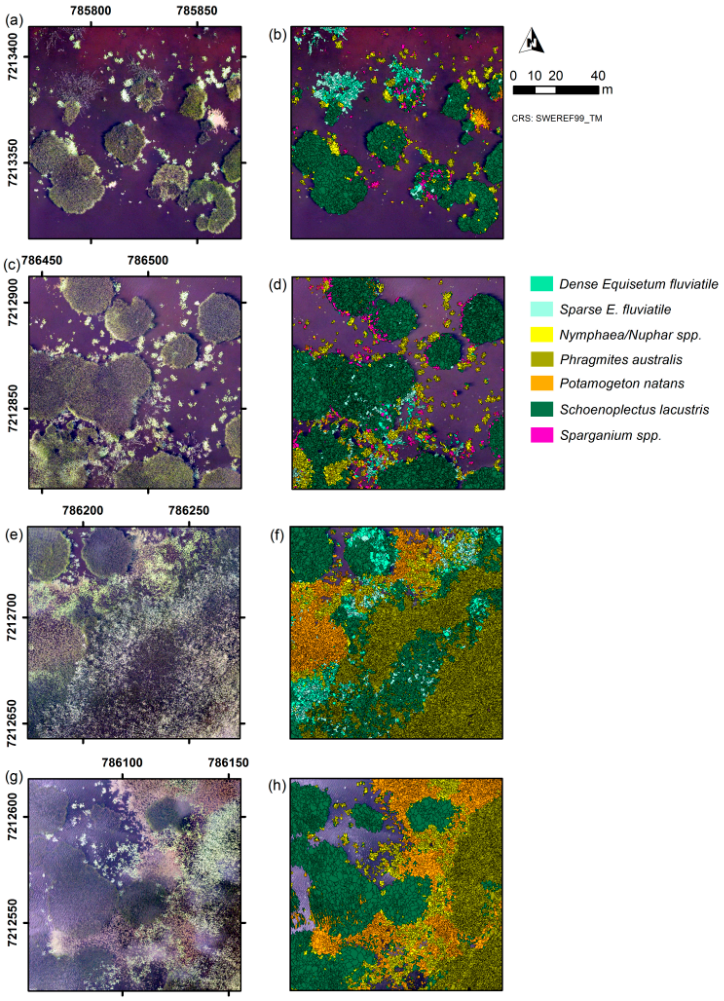

Figure 2. True-colour orthoimage and dominant-taxon classification based on height data combined with spectral and textural features of test sites I (**a** and **b**), II (**c** and **d**), IV (**e** and **f**), and V (**g** and **h**).

Producer's and User's accuracies at the dominant-taxon level varied between classes and sites (Table 4). For the majority of classes and sites, Producer's and User's accuracies increased when height data were included (Table 4), and the overall increases of segment- and area-based Producer's and User's accuracies were statistically significant (T and p values given in Table 5). The class of *P. australis* (emergent, present at Sites IV and V) showed the largest increase of Producer's accuracy (Table 4). At Site IV, the reduced confusion of all taxa with *P. australis* resulted in increased User's accuracies ($\geq$12%) for all classes except for dense *E. fluviatile* which increased by only 1% (Tables 4 and S1). Also at Site IV, the confusion between floating-leaved *P. natans* and emergent *S. lacustris* was reduced (Table S1). At Site V, mainly the confusion between floating-leaved *Nymphaea*/*Nuphar* spp. and emergent *P. australis* was reduced (Table S1). At Sites I and II, the confusion of emergent *S. lacustris* with all other taxa was reduced (Table S1). In the study based on spectral and textural features alone, the two *E. fluviatile* classes, *P. natans* and *Sparganium* spp., in all cases had a lower User's accuracy than Producer's accuracy, indicating a large number of false inclusions [2]. The inclusion of height data reduced most differences between the User's and Producer's accuracies, but User's accuracies were still lower than Producer's accuracies in all cases except for sparse *E. fluviatile* at Site III (Table 4). For the two classes that were most reliably classified without height data, *Nymphaea*/*Nuphar* spp. and *S. lacustris*, the inclusion of height data further increased both Producer's and User's accuracies at all sites (generally between 0.3% and 44%; Table 4).

Table 3. Producer's and User's accuracy (%, segment-, and area-based), number of validation segments, and total area of validation segments (m^2) for the classification of growth-forms based on height data combined with spectral and textural features presented by test site and class: water (W), nymphaeid (N), and helophyte (H). For comparison, the results from our previous study [2] based on spectral and textural features alone were reproduced in this table. Bold numbers indicate a statistically significant increase when height data were included and stars indicate the level of significance (* for $\alpha < 0.025$, ** for $\alpha < 0.005$, and *** for $\alpha < 0.0005$). Valid *N* is the total number of differences with either a positive or negative sign.

	Site I			**Site II**			**Site III**			**Site IV**			**Site V**			**Wilcoxon Signed-Rank Test**		
	W	**N**	**H**	**W**	**N**	**H**	**W**	**N**	**H**	**W**	**N**	**H**	**W**	**N**	**H**	**Valid *N***	***T***	***p***
Producer's accuracy (segment-based)																		
Height, spectral, and textural features	**83**	**88**	**84**	**89**	**68**	**95**	**65**	**83**	**75**	**90**	**90**	**74**	**93**	**88**	**65**	12	0	**0.002** **
Spectral and textural features	81	82	79	89	59	92	63	78	69	90	82	49	93	68	53			
User's accuracy (segment-based)																		
Height, spectral, and textural features	**98**	**65**	**88**	**86**	**94**	**86**	**83**	**93**	**43**	**25**	**58**	**98**	**38**	**88**	**87**	14	11	**0.009** *
Spectral and textural features	97	58	84	89	84	82	85	92	35	25	33	92	39	74	63			
No. of validation segments	106	68	176	57	87	206	52	246	52	10	71	274	28	163	159			
Producer's accuracy (area-based)																		
Height, spectral, and textural features	**97**	**87**	**89**	**96**	**63**	**96**	**90**	**74**	**80**	**92**	**89**	**73**	**96**	**86**	**62**	12	0	**0.002** **
Spectral and textural features	97	83	87	96	54	96	89	70	68	92	77	49	96	69	56			
User's accuracy (area-based)																		
Height, spectral, and textural features	**99**	**64**	**91**	**96**	**94**	**90**	**90**	**93**	**58**	**35**	**57**	**98**	**32**	**93**	**88**	15	8	**0.003** **
Spectral and textural features	99	59	89	97	89	88	87	92	49	35	30	92	34	80	73			
Total area of validation segments	458	37	177	162	39	176	145	121	66	18	42	201	30	120	168			

Table 4. Producer's and User's accuracy (%, segment-, and area-based), number of validation segments, and total area of validation segments (m^2) for the classification of dominant taxa based on height data combined with spectral and textural features for Sites I–V presented by vegetation class. For comparison, the results from our previous study [2] based on spectral and textural features alone were reproduced in this table. Vegetation classes have been abbreviated as follows: *Equisetum fluviatile* (*E.f.*), *Nymphaea*/*Nuphar* spp. (*N./N.* spp.), *Phragmites australis* (*P.a.*), *Potamogeton natans* (*P.n.*), *Schoenoplectus lacustris* (*S.l.*), and *Sparganium* spp. (*S.* spp.). Bold and italic numbers indicate an increase of ≥5% when height data were included.

	Vegetation Class					
	Sparse *E.f.*	**Dense *E.f.***	***N./N.* spp.**	***P.a.***	***P.n.***	***S.l.***	***S.* spp.**
Site I						
Producer's accuracy (segment-based)						
Height, spectral, and textural features	60	***56***	83	80	***83***	***50***
Spectral and textural features	60	48	79	80	68	40
User's accuracy (segment-based)						
Height, spectral, and textural features	45	***44***	***93***	***53***	***97***	***16***
Spectral and textural features	41	33	78	47	92	11
No. of validation segments	15	27	95	10	206	10
Producer's accuracy (area-based)						
Height, spectral, and textural features	76	43	86	91	***87***	***48***
Spectral and textural features	76	41	83	91	74	31
User's accuracy (area-based)						
Height, spectral, and textural features	***38***	***49***	***91***	***72***	98	***13***
Spectral and textural features	33	33	71	66	95	8
Total area of validation segments	12	24	50	10	214	5
Site II						
Producer's accuracy (segment-based)						
Height, spectral, and textural features	50	***80***	71	20	***90***	70
Spectral and textural features	50	70	70	20	65	70
User's accuracy (segment-based)						
Height, spectral, and textural features	***21***	***47***	***93***	***11***	***97***	***35***
Spectral and textural features	12	29	84	6	92	27
No. of validation segments	10	10	90	10	230	10
Producer's accuracy (area-based)						
Height, spectral, and textural features	63	61	73	13	***91***	72
Spectral and textural features	63	59	71	13	72	72
User's accuracy (area-based)						
Height, spectral, and textural features	***26***	***44***	***89***	5	99	***33***
Spectral and textural features	15	18	81	3	96	23
Total area of validation segments	7	4	40	4	205	5

Table 4. *Cont.*

	Vegetation Class						
	Sparse *E.f.*	**Dense *E.f.***	***N./N.* spp.**	***P.a.***	***P.n.***	***S.l.***	***S.* spp.**
Site III							
Producer's accuracy (segment-based)							
Height, spectral, and textural features	50	59	70		50		70
Spectral and textural features	48	59	66		50		70
User's accuracy (segment-based)							
Height, spectral, and textural features	***54***	28	95		13		30
Spectral and textural features	44	24	94		13		32
No. of validation segments	40	22	273		12		10
Producer's accuracy (area-based)							
Height, spectral, and textural features	64	71	61		72		67
Spectral and textural features	62	71	57		72		67
User's accuracy (area-based)							
Height, spectral, and textural features	***80***	***37***	95		18		36
Spectral and textural features	75	32	95		20		38
Total area of validation segments	61	22	131		11		7
Site IV							
Producer's accuracy (segment-based)							
Height, spectral, and textural features	***90***	20	***66***	***100***	***94***	***59***	
Spectral and textural features	80	40	61	48	88	43	
User's accuracy (segment-based)							
Height, spectral, and textural features	***30***	10	***87***	***93***	***79***	***97***	
Spectral and textural features	17	9	68	81	38	69	
No. of validation segments	10	10	41	170	33	100	
Producer's accuracy (area-based)							
Height, spectral, and textural features	***98***	13	59	***100***	***96***	***74***	
Spectral and textural features	92	23	56	43	89	51	
User's accuracy (area-based)							
Height, spectral, and textural features	***32***	12	***82***	***95***	***82***	***96***	
Spectral and textural features	19	11	70	83	34	77	
Total area of validation segments	9	12	22	95	22	97	
Site V							
Producer's accuracy (segment-based)							
Height, spectral, and textural features			***95***	***100***	76	74	
Spectral and textural features			55	53	78	73	
User's accuracy (segment-based)							
Height, spectral, and textural features			***83***	***89***	***85***	84	
Spectral and textural features			49	53	79	80	
No. of validation segments			78	85	96	91	
Producer's accuracy (area-based)							
Height, spectral, and textural features			***93***	***100***	77	85	
Spectral and textural features			49	62	79	84	
User's accuracy (area-based)							
Height, spectral, and textural features			***82***	***83***	***87***	89	
Spectral and textural features			53	57	77	87	
Total area of validation segments			41	51	89	134	

Table 5. Valid *N*-, *T*-, and *p*-values from one-sided Wilcoxon matched pairs signed-rank tests for Producer's and User's accuracy (segment- and area-based) at the dominant taxon level for all classes and sites combined. Bold numbers indicate a statistically significant increase when height data were included and stars indicate the level of significance (* for $\alpha < 0.025$, ** for $\alpha < 0.005$, and *** for $\alpha < 0.0005$). Valid *N* is the total number of differences with either a positive or negative sign.

	Valid *N*	*T*	*p*
Producer's accuracy (segment-based)	19	18	**0.00194** **
User's accuracy (segment-based)	27	5	**0.00001** ***
Producer's accuracy (area-based)	20	20	**0.00151** **
User's accuracy (area-based)	27	8	**0.00001** ***

4. Discussion

When height data from a UAS-DSM were included in the classification along with spectral and textural features from a UAS-orthoimage, the classification accuracy was higher than when spectral and textural features alone were used. The inclusion of height data successfully reduced the confusion between taxa that belonged to different growth forms (emergent and floating-leaved). In contrast to the study based on spectral and textural features alone [2], where emergent *P. australis* was confused with all other taxa, it now belonged to the most reliably classified taxa. *P. australis* was the tallest taxa in our classification [3]. It has a bright green colour (similar to *Nymphaea*/*Nuphar* spp., *Sparganium* spp., and sun exposed *S. lacustris*) which is easy to detect against a darker background of, for example, dark green vegetation or water.

In the previous study [2], the classification of *S. lacustris* was also problematic due to the high variation in spectral appearance within this taxon. Typically, at the edge of stands of *S. lacustris*, stems are bent and more exposed to the sun than those in the interior of the stands. This results in the former looking more brightly green than the majority of *S. lacustris* stems. In addition, we observed areas with low cover within *S. lacustris* stands, where stems were probably straighter than the majority of *S. lacustris* stems; these areas appeared darker. Therefore, in the classification based on spectral and textural features alone, *S. lacustris* was often confused with other taxa which decreased the User's accuracy, especially of taxa that covered smaller total areas than the relatively common *S. lacustris*. With the inclusion of height data, the classification of *S. lacustris* was more reliable.

Compared to the other two emergent taxa, *E. fluviatile* was the least affected by the inclusion of height data. *E. fluviatile* had the lowest vegetation height among the emergent taxa in this study [3]. The two *E. fluviatile* classes were mainly confused with each other and *S. lacustris* (also emergent) but, especially at Site III it was also confused with *Nymphaea*/*Nuphar* spp. (floating-leaved). The inclusion of height data could not substantially reduce the confusion between these classes even though they belong to different growth forms. *E. fluviatile* has a straight, needle-like shape, and the fine leaves are also needle-like and were almost invisible on the UAS-images. At Site III, *E. fluviatile* rarely formed stands that were dense enough to completely obscure the water surface and formed to a large extent mixed vegetation stands with *Nymphaea*/*Nuphar* spp. This probably led to a larger variation in mean height values for *E. fluviatile*-covered segments at this site. In our previous study, we found that Site III had the highest proportion of misclassifications where a non-dominant taxon was wrongly classified as the dominant taxon. *E. fluviatile* was the only emergent taxa present at Site III, which explains the relatively small increase in classification accuracy at this test site.

The addition of height data also helped to reduce the confusion among emergent taxa, for example, between *P. australis* and *S. lacustris* (Sites IV and V), between *P. australis* and *E. fluviatile* (Site IV), and between *S. lacustris* and *E. fluviatile* (Sites I, II, and IV). This indicates that the UAS-DSM successfully resolved even smaller differences in vegetation height than between emergent and floating-leaved taxa.

The reduced confusion among growth forms and taxa resulted in very good classification accuracies (at least ~80%) at most test sites, both at the growth-form and the dominant-taxon level, including the site with the largest vegetation complexity. At Site V, the test site with low image

quality, the overall classification accuracy increased, indicating that the inclusion of height data further increased the robustness of the classification process. These results show good potential for operative mapping and monitoring of aquatic vegetation at a high level of thematic detail and in an automated way, which is important to time-efficiently cover larger areas.

Conventional orthoimage production is often based on less dense point clouds from which objects with heights above ground level such as vegetation or buildings are removed. Our suggested method requires the production of true orthoimages with unfiltered dense point clouds (ca. >100 points per m^2). This implies increased operator time and computational costs compared to conventional orthoimages. Thanks to recent developments in digital photogrammetry and computer vision, an increasing number of user-friendly software programmes for UAS-image processing are available. The calculation of 3D point clouds from overlapping UAS-images is usually integrated in the workflow of these programmes and is typically part of the production of a true UAS-orthoimage with high spatial accuracy. The height information from image-based dense point clouds generated with Structure-from-Motion software based on algorithms such as Semi-Global Matching [27] can be comparable to that from airborne LiDAR [28] and even low-cost systems such as a UAS equipped with a consumer grade camera allow for surface reconstructions of high quality when the image overlap is high [29]. Once a dense point cloud is constructed, the production of a UAS-DSM is only a minor effort. Regarding the high increase in accuracy achieved in our study, UAS-DSMs have a large potential to efficiently improve the classification results when combined with spectral data.

For our study, UAS-DSMs for the test sites were produced after the original UAS-orthoimage production and independent from the orthoimage. This was done because the original UAS-orthoimage was produced by an external image processing company and the point cloud was not initially made available for our study. The independent production of the UAS-orthoimage and UAS-DSMs resulted in a spatial displacement between the two, which is a potential source of error in our classification. The spatial displacement varied from site to site but had an average of 4.5 cm, and a maximum of 5.6 cm, which is about the size of one pixel (5 cm). For future studies, we recommend producing the UAS-DSM together with the UAS-orthoimage to avoid differences in data co-registration.

Ground control points with height measurements were missing in our study. This was solved by using the water surface as the zero level. In our study, the internal relative differences in vegetation height were most important since our focus was on the classification of different growth-forms with relatively large differences in vegetation height. The maximum vegetation heights in the UAS-DSMs of the five test sites are plausible. However, when the UAS-DSM is to be used for the extraction of absolute height values, for example, for biomass estimation, height measurements of reference points in the field are recommended for calibration.

5. Conclusions

At five test sites with varying vegetation complexity and image quality at a lake in northern Sweden, the inclusion of height data in addition to spectral and textural features from a true-colour UAS-orthoimage with 5-cm pixels significantly increased the classification accuracy of non-submerged aquatic vegetation as compared to using spectral and textural features alone. The inclusion of height data reduced the confusion between taxa that appeared similar in the image but belonged to different growth forms (emergent and floating-leaved), as well as among emergent taxa. The overall classification accuracy increased to at least ~80% at all five test sites for growth forms and at four out of five test sites for dominant taxa. The combination of true-colour UAS-orthoimages with height data derived from dense 3D point clouds from image matching has a large potential to efficiently increase the accuracy of automated classification. This approach improves the possibilities for operative mapping and monitoring of non-submerged aquatic vegetation at a high level of thematic detail covering larger areas such as entire lakes.

Supplementary Materials: The following are available online at www.mdpi.com/2072-4292/9/3/247/s1, Figure S1: Field images of taxa present at Ostträsket, Table S1: Error matrices for all test sites at all levels of thematic detail and differences between error matrices from the classifications with and without height data.

Acknowledgments: We thank Jonas Bohlin and Olle Hagner for technical support and advice regarding DSM production. This work was funded by the Swedish Research Council Formas (reference number 2014-1425), and was conducted as part of the European project ImpactMin (project number 244166 in FP7-ENV-2009-1) as well as the research programme WATERS, funded by the Swedish Environmental Protection Agency (Dnr 10/179) and Swedish Agency for Marine and Water Management.

Author Contributions: All authors conceived and designed the study; E.H. derived the digital surface models and analysed the image data; E.H. wrote the paper with the contributions of H.R. and F.E.

Conflicts of Interest: The authors declare no conflict of interest.

Abbreviations

The following abbreviations are used in this article:

DSM	Digital surface model
LiDAR	Light detection and ranging
OBIA	Object-based image analysis
PAMS	Personal Aerial Mapping System
RGB	Red green blue
3D	Three-dimensional
UAS	Unmanned aircraft system

References

1. Anderson, K.; Gaston, K.J. Lightweight unmanned aerial vehicles will revolutionize spatial ecology. *Front. Ecol. Environ.* **2013**, *11*, 138–146. [CrossRef]
2. Husson, E.; Ecke, F.; Reese, H. Comparison of manual mapping and automated object-based image analysis of non-submerged aquatic vegetation from very-high-resolution UAS images. *Remote Sens.* **2016**, *8*, 724. [CrossRef]
3. Mossberg, B.; Stenberg, L. *Den Nya Nordiska Floran*; Wahlström & Widstrand: Aurskog, Norge, 2006.
4. Tempfli, K.; Kerle, N.; Huurneman, G.C.; Janssen, L.L.E. *Principles of Remote Sensing*; ITC: Enschede, The Netherlands, 2009.
5. Colwell, R. *Manual of Photographic Interpretation*; American Society of Photogrammetry: Washington, DC, USA, 1960.
6. Madden, M.; Jordan, T.; Bernardes, S.; Cotten, D.L.; O'Hare, N.; Pasqua, A. Unmanned aerial systems and structure from motion revolutionize wetlands mapping. In *Wetlands: Applications and Advances*; Tiner, R.W., Lang, M.W., Klemas, V.V., Eds.; CRC Press: Boca Raton, FL, USA, 2015; pp. 195–219.
7. Colomina, I.; Molina, P. Unmanned aerial systems for photogrammetry and remote sensing: A review. *ISPRS J. Photogramm. Remote Sens.* **2014**, *92*, 79–97. [CrossRef]
8. Cunliffe, A.M.; Brazier, R.E.; Anderson, K. Ultra-fine grain landscape-scale quantification of dryland vegetation structure with drone-acquired structure-from-motion photogrammetry. *Remote Sens. Environ.* **2016**, *183*, 129–143. [CrossRef]
9. Ke, Y.H.; Quackenbush, L.J.; Im, J. Synergistic use of Quickbird multispectral imagery and Lidar data for object-based forest species classification. *Remote Sens. Environ.* **2010**, *114*, 1141–1154. [CrossRef]
10. Nordkvist, K.; Granholm, A.-H.; Holmgren, J.; Olsson, H.; Nilsson, M. Combining optical satellite data and airborne laser scanner data for vegetation classification. *Remote Sens. Lett.* **2012**, *3*, 393–401. [CrossRef]
11. Granholm, A.H.; Olsson, H.; Nilsson, M.; Allard, A.; Holmgren, J. The potential of digital surface models based on aerial images for automated vegetation mapping. *Int. J. Remote Sens.* **2015**, *36*, 1855–1870. [CrossRef]
12. Reese, H.; Nordkvist, K.; Nyström, M.; Bohlin, J.; Olsson, H. Combining point clouds from image matching with Spot 5 multispectral data for mountain vegetation classification. *Int. J. Remote Sens.* **2015**, *36*, 403–416. [CrossRef]
13. Reese, H.; Nyström, M.; Nordkvist, K.; Olsson, H. Combining airborne laser scanning data and optical satellite data for classification of alpine vegetation. *Int. J. Appl. Earth Obs. Geoinf.* **2014**, *27*, 81–90. [CrossRef]

14. Gillan, J.K.; Karl, J.W.; Duniway, M.; Elaksher, A. Modeling vegetation heights from high resolution stereo aerial photography: An application for broad-scale rangeland monitoring. *J. Environ. Manag.* **2014**, *144*, 226–235. [CrossRef] [PubMed]
15. Rampi, L.P.; Knight, J.F.; Pelletier, K.C. Wetland mapping in the upper midwest United States: An object-based approach integrating Lidar and imagery data. *Photogramm. Eng. Remote Sens.* **2014**, *80*, 439–448. [CrossRef]
16. Al-Rawabdeh, A.; He, F.N.; Moussa, A.; El-Sheimy, N.; Habib, A. Using an unmanned aerial vehicle-based digital imaging system to derive a 3D point cloud for landslide scarp recognition. *Remote Sens.* **2016**, *8*, 95. [CrossRef]
17. Vetrivel, A.; Gerke, M.; Kerle, N.; Vosselman, G. Segmentation of UAV-based images incorporating 3D point cloud information. In Proceedings of the Joint ISPRS Conference on Photogrammetric Image Analysis (PIA) and High Resolution Earth Imaging for Geospatial Information (HRIGI), Munich, Germany, 25–27 March 2015.
18. Lechner, A.M.; Fletcher, A.; Johansen, K.; Erskine, P. Characterising upland swamps using object-based classification methods and hyper-spatial resolution imagery derived from an umanned aerial vehicle. In Proceedings of the XXII ISPRS Congress, Melbourne, Australia, 25 August–1 September 2012.
19. Kuria, D.N.; Menz, G.; Misana, S.; Mwita, E.; Thamm, H.; Alvarez, M.; Mogha, N.; Becker, M.; Oyieke, H. Seasonal vegetation changes in the Malinda wetland using bi-temporal, multi-sensor, very high resolution remote sensing data sets. *Adv. Remote Sens.* **2014**, *3*, 33–48. [CrossRef]
20. Tamminga, A.; Hugenholtz, C.; Eaton, B.; Lapointe, M. Hyperspatial remote sensing of channel reach morphology and hydraulic fish habitat using an unmanned aerial vehicle (UAV): A first assessment in the context of river research and management. *River Res. Appl.* **2015**, *31*, 379–391. [CrossRef]
21. Boon, M.A.; Greenfield, R.; Tesfamichael, S. Wetland assessment using unmanned aerial vehicle (UAV) photogrammetry. In Proceedings of the XXIII ISPRS Congress, Prague, Czech Republic, 12–19 July 2016.
22. Congalton, R.G. A review of assessing the accuracy of classifications of remotely sensed data. *Remote Sens. Environ.* **1991**, *37*, 35–46. [CrossRef]
23. Pontius, R.G.; Millones, M. Death to kappa: Birth of quantity disagreement and allocation disagreement for accuracy assessment. *Int. J. Remote Sens.* **2011**, *32*, 4407–4429. [CrossRef]
24. Olofsson, P.; Foody, G.M.; Herold, M.; Stehman, S.V.; Woodcock, C.E.; Wulder, M.A. Good practices for estimating area and assessing accuracy of land change. *Remote Sens. Environ.* **2014**, *148*, 42–57. [CrossRef]
25. Radoux, J.; Bogaert, P.; Fasbender, D.; Defourny, P. Thematic accuracy assessment of geographic object-based image classification. *Int. J. Geogr. Inf. Sci.* **2011**, *25*, 895–911. [CrossRef]
26. Zar, J.H. *Biostatistical Analysis*; Prentice-Hall Inc.: Upper Saddle River, NJ, USA, 1999.
27. Hirschmüller, H. Stereo processing by semi-global matching and mutual information. *IEEE Trans. Pattern Anal. Mach. Intell.* **2008**, *30*, 328–341. [CrossRef] [PubMed]
28. Leberl, F.; Irschara, A.; Pock, T.; Meixner, P.; Gruber, M.; Scholz, S.; Wiechert, A. Point clouds: Lidar versus 3D vision. *Photogramm. Eng. Remote Sens.* **2010**, *76*, 1123–1134. [CrossRef]
29. Haala, N.; Cramer, M.; Rothermel, M. Quality of 3D point clouds from highly overlapping UAV imagery. In Proceedings of the Conference on Unmanned Aerial Vehicles in Geomatics (UAV-g), Rostock, Germany, 4–6 September 2013.